

Canny Algorithm, Cosmic Strings and the Cosmic Microwave Background

Rebecca J. Danos and Robert H. Brandenberger

Department of Physics, McGill University, Montréal, QC, H3A 2T8, Canada

(Dated: September 12, 2018)

We describe a new code to search for signatures of cosmic strings in cosmic microwave anisotropy maps. The code implements the Canny Algorithm, an edge detection algorithm designed to search for the lines of large gradients in maps. Such a gradient signature which is coherent in position space is produced by cosmic strings via the Kaiser-Stebbins effect. We test the power of our new code to set limits on the tension of the cosmic strings by analyzing simulated data with and without cosmic strings. We compare maps with a pure Gaussian scale-invariant power spectrum with maps which have a contribution of a distribution of cosmic strings obeying a scaling solution. The maps have angular scale and angular resolution comparable to what current and future ground-based small-scale cosmic microwave anisotropy experiments will achieve. We present tests of the codes, indicate the limits on the string tension which could be set with the current code, and describe various ways to refine the analysis. Our results indicate that when applied to the data of ongoing cosmic microwave experiments such as the South Pole Telescope project, the sensitivity of our method to the presence of cosmic strings will be more than an order of magnitude better than the limits from existing analyses.

PACS numbers: 98.80.Cq

I. INTRODUCTION

There has been a recent renaissance of interest in cosmic strings (see e.g [1]) as a mechanism contributing to the spectrum of primordial cosmological perturbations and the corresponding anisotropies in cosmic microwave anisotropy (CMB) maps. In part this renewed interest is sparked by the realization that many supergravity models of inflation also lead to the production of strings at the end of the period of inflation [2]. In addition, many models of inflation in the context of string theory predict the formation of a network of strings at the end of the inflationary phase [3]. The conditions under which these cosmic superstrings [4] are stable have been explored in [5]. Cosmic superstrings may also arise in other approaches to superstring cosmology such as the Ekpyrotic scenario [6] or string gas cosmology [7, 8].

If matter is described by a particle physics model which admits stable strings forming after inflation, then by causality it is inevitable that a network of such strings will form during the cosmological phase transition which corresponds to the symmetry breaking which is responsible for the existence of the strings [9]. It is inevitable that the network of strings contains “infinite” strings (strings crossing the entire volume). For applications in cosmology one divides the strings into “loops” (loops of cosmic string with a curvature radius smaller than the Hubble radius $H^{-1}(t)$, where $H(t)$ is the cosmological expansion rate) and “long strings” (infinite strings and loops with curvature radius larger than the Hubble radius). The causality argument [9] (see also [10–12] for some standard reviews on cosmic strings and structure formation, and [13] for the original references) implies, in fact, that at all times after the phase transition a network of long strings with a correlation length (mean curvature radius) comparable or smaller than the Hubble radius will sur-

vive. It can be argued [10–12, 14] that a network of (non-superconducting) strings will approach a “scaling solution” for which at all late times t the correlation length of the network of long strings is a fixed fraction of the Hubble radius¹.

Cosmic strings [24] are described by their mass per unit length μ which is usually quoted in terms of the dimensionless number $G\mu$, G being Newton’s gravitational constant. A straight string has a tension which is equal in magnitude to μ . Hence, the effective action which describes the motion of a straight string is the Nambu-Goto action, the same action which describes fundamental strings. Since cosmic strings carry energy, they will lead to density fluctuations and cosmic microwave background (CMB) anisotropies.

The network of cosmic strings will generate a scale-invariant spectrum of cosmological perturbations [25]. More relevant to the current paper, cosmic strings generate a very specific signature in cosmic microwave background anisotropy maps, namely line discontinuities [26]. These line discontinuities arise since space perpendicular to a cosmic string is a cone with deficit angle given by [27]

$$\alpha = 8\pi G\mu. \quad (1)$$

Since the motion of cosmic strings is relativistic, photons passing on different sides of the string moving with a velocity v perpendicular to the plane spanned by the string

¹ It is likely that the distribution of cosmic string loops also approaches a scaling solution; see e.g [15–17] for early simulations of cosmic string networks supporting the conclusion that the distribution of loops also scales, [18] for an opposing view based on field theory simulations and [19–23] for more recent work supporting scaling for string loops.

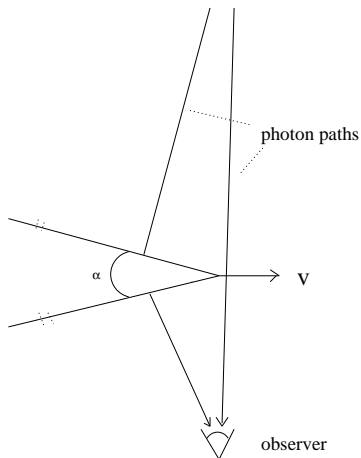


FIG. 1: Geometry of the Kaiser-Stebbins effect: Photons passing on the two sides of the moving cosmic string obtain a relative Doppler shift for the observer who is at rest.

direction and the line of sight between the observer and the string will be seen by the observer with a relative Doppler shift

$$\frac{\delta T}{T} = 8\pi\gamma(v)vG\mu, \quad (2)$$

where $\gamma(v)$ is the relativistic gamma factor (see Figure 1). Looking in direction of the string, we will see a line in the sky across which the CMB temperature jumps by the above amount. We will denote this effect, the Kaiser-Stebbins effect, as the KS effect in the rest of the paper.

The conical deformation of space induced by a “long” cosmic string has a length of the order the Hubble radius, i.e. of the order of t in direction of the string. Since cosmic strings are formed in a phase transition and the effects of the transition travel with the speed of light, the depth of the region affected by the string (in direction perpendicular to the string) is t , as shown in [28]. Hence, each string between t_{rec} and t_0 whose “zone of influence”² is intersected by the past light cone of the observer will induce a line discontinuity in the CMB temperature map with length gt , where g is a random number in the interval $0 < g < 1$ which takes into account the random angle of the velocity vector of the string relative to the plane determined by the string direction and the observer’s line of sight to the string. The anisotropy pattern induced by a single string segment contains several edges. There is the central line discontinuity (2) coming from photons which pass on different sides of the string. Since the deficit angle in Figure 1 has finite depth (in direction $-v$), as explained in the previous paragraph there will be two edges (again sharp because the deficit angle sharply decreases to zero [28]) with half the value of δT .

Finally, our modelling of the string network in terms of straight segments introduces the sharp “boundary” edges perpendicular to the central edge (see also Figure 3).

To detect the line discontinuities in CMB maps produced by cosmic strings, it is important to have small angular resolution. Strings present in the universe between the time of last scattering and the present time contribute to the signal. However, according to the cosmic string scaling solution, the most numerous strings are those present at or shortly after last scattering. The Hubble radius at that time subtends an angle of about 1.8° . If the angular resolution is not much smaller than this angle, then the anisotropies produced by these strings will not be distinguishable from anisotropies produced by Gaussian noise with the corresponding coherence length. On the other hand, full sky coverage is not essential. Thus, ground-based small angular resolution surveys such as ACT [29] or the South Pole Telescope [30] both of which have angular resolution of about $1'$ are ideal to search for strings. The Planck satellite experiment [31] with an angular resolution of about $5'$ will also yield a good data set to use, in particular since the systematic errors in the data will likely be smaller.

The KS effect is a part of the “Integrated Sachs-Wolfe” [32] contribution to CMB anisotropies. The primordial cosmological fluctuations produced by strings also contribute to the regular Sachs-Wolfe effect. In contrast to cosmological fluctuations produced in inflationary cosmology, those produced by cosmic strings are “incoherent” and “active” as opposed to “coherent” and “passive” [33]. The string network is continuously seeding growing curvature fluctuations on super-Hubble scales, and therefore the fluctuations enter the Hubble radius not as standing waves. As a consequence, the angular power spectrum of CMB anisotropies does not have [34–36] the acoustic ringing associated with coherent passive fluctuations [37]. Since acoustic ringing has been observed with recent high precision CMB measurements [38, 39], it is now clear that cosmic strings cannot be the main source of cosmological fluctuations. Their contribution is bounded from the accurate measurements of the angular power spectrum of the CMB in the region of the first acoustic peak to be less than 10% [40] which corresponds to a value of $G\mu$ of about 3×10^{-7} . In the literature, one finds slightly stronger constraints which come from pulsar timing data [41, 42]. However, pulsar bounds make use of estimates of the spectrum of gravitational radiation from cosmic string loops. Since there is still a lot of uncertainty about the distribution of cosmic string loops, and since the amount of gravitational radiation from a fixed loop is also rather uncertain, bounds on $G\mu$ coming from millisecond pulsar timing are not very robust. Much more robust signatures come from the long and straight strings, signatures which we are discussing in this paper.

Early work to identify the KS signal of cosmic strings in CMB anisotropy maps was presented in [43] which concluded that the angular resolution of WMAP would

² By which we mean the region of space which is deformed due to the presence of the string.

not be small enough to resolve the KS signature. After the release of the WMAP data [39], there were two sets of analyses introducing new algorithms to look specifically for the KS signature. Lo and Wright [44] applied a matched filtering method, whereas Jeong and Smoot [45] introduced new statistics such as one measuring the connectedness of neighboring temperature steps or another one proposing a decomposition of the temperature map into constant, Gaussian and straight string step components. Both groups applied their statistics to the WMAP data. From the null results of the searches, a direct upper bound on the string tension of $G\mu < 10^{-6}$ could be set, a bound not competitive with the existing bounds from the matching of the angular power spectrum.

In [46], it was proposed to make use of the Canny algorithm [47] to search for the KS effect, and the preliminary analysis showed that the statistic offers the promise to improve the limit on $G\mu$ from direct searches for the KS signal by a large factor. The Canny algorithm is an edge detection algorithm which was previously used in image recognition work and metallurgy. It looks for lines in a map across which there is a large gradient. Thus, the algorithm appears to be well suited to detect the KS signature. In this paper we present a new and improved implementation of the Canny algorithm and apply it to test data. In agreement with [46] (and with the followup paper [48]), we find the new analysis based on the Canny algorithm is able to find or rule out strings with a tension greater than an upper bound which is more than an order of magnitude smaller than previous bounds derived from looking for the KS signature of strings. We emphasize that the code on which this paper is based was developed completely independently from that used in [46] and [48]. It is different in structure and in fact is based on a different programming language. The fact that the results reported here agree with those in [48] presents a very important check on the methods.

The Canny algorithm works in position space. Starting from an anisotropy map, it first produces an “edge map”, the edges corresponding to lines in the sky perpendicular to which the gradient of the anisotropy map is sufficiently large³. The edge detection algorithm must be able to take into account the fact that Gaussian noise superimposed on top of the cosmic string signal will produce large variations in the magnitude of the gradient along a cosmic string edge. Given the edge map, a second algorithm counts the number of edges of fixed length and produces a histogram of edge lengths. Both the edge detection and the edge counting algorithms contain various parameters and thresholds which can be set by the user and which can be tuned to give the algorithm maximal discriminatory power, and are improved over the original code presented in [46]. The values of the thresholds and

parameters will depend on the specific data. The final step of the code is a statistical comparison between the histograms produced in the previous step for data with and without cosmic strings.

The outline of this paper is as follows: In the following section we discuss the construction of the test data maps - both the pure Gaussian maps and the maps containing cosmic strings. In Section 3 we present the new implementation of the Canny algorithm. We first describe the algorithm which takes the CMB temperature map and converts it into an edge map. Then, we turn to the separate algorithm which is used to produce a histogram of edge lengths. Section 4 presents the results from the application of the Canny algorithm to the test maps. We conclude with a summary of the method and results, focusing on refinements of the code which can be made to improve the code’s discriminatory power, and give a preview of future applications.

II. SIMULATIONS

In this section we describe the codes which were used to create the simulated temperature maps. The maps have two components, firstly a Gaussian map with an angular power spectrum corresponding to the inflationary “concordance model”, the second a map of anisotropies produced by long cosmic strings according to the KS effect. These simulation routines have been created from scratch, without using any input from the existing code [46]. The simulation routines are written in Interactive Data Language (IDL). Both for the inflationary fluctuations and the cosmic string maps, the theory predicts ensemble averages from which particular classical realizations are drawn. To obtain firm predictions, a large number of simulations must therefore be run.

Since we have in mind applying our code to surveys with small angular resolution but only partial sky coverage, we work in the “flat sky” approximation [49] in which a segment of the sky is approximated by a rectangle. This approximation is made because of computational ease, since the basis solutions of the wave equation in flat space, the Fourier modes, are much easier to work with than the basis functions on a sphere, the spherical harmonics.

A. Gaussian Map

First we create a square grid temperature map of the Gaussian inflationary perturbations. The grid size is set by the angular resolution and by the angular size of the survey which we want to simulate (the number of grid points along an axis is $N_{max} = L/R$, where L is the extent of the survey along the axis being considered, and R is the angular resolution). The map is constructed based on the angular power spectrum of CMB fluctuations computed using one of the standard codes used in

³ As detailed in Section 3, a new aspect of the present code is to search for gradients in a range tuned to the expected KS signal.

the literature (see below).

A differential temperature value, $\Delta T/T$, (corresponding to the temperature with the monopole subtracted) is assigned to each grid point (n, m) (n and m are integers) of the map, where each grid point represents a position in the window of the observed sky. If L is the length of a side of the window of observation in degrees in the first coordinate direction, then the angular distance of a grid point (n, m) from the edge is $x = nL/N_{max}$. The two dimensional vector is designated by \mathbf{x} .

The code is designed to construct a square grid. If rectangular areas are needed, we can construct a larger square temperature map and cut out the appropriate rectangle from this larger grid. The applicable scales are less than 60° indicating the applicability of the ‘‘flat sky’’ approximation.

In general, the temperature anisotropy of the CMB is expressed in terms of spherical harmonics $Y_{lm}(\theta, \phi)$, θ and ϕ being latitude and longitude, respectively:

$$\frac{\Delta T}{T}(\theta, \phi) = \sum_{l,m} a_{lm} Y_{lm}(\theta, \phi) \quad (3)$$

where a_{lm} are the coefficients of the expansion. However, since the observed window will be less than 60 degrees (we will take it to be approximately 10 degrees), plane waves can be substituted for Y_{lm} per the flat sky approximation:

$$\frac{\Delta T}{T}(\mathbf{x}) = \sum_{\mathbf{k}} T(\mathbf{k}) e^{i\mathbf{k}\cdot\mathbf{x}}. \quad (4)$$

(N.B. In the following equations $T(\mathbf{x}) = \Delta T(\mathbf{x})/T$ and $T(\mathbf{k}) = \Delta T(\mathbf{k})/T$) Comparing these equations, it is obvious that the coefficients $T(\mathbf{k})$ correspond to a_{lm} so that:

$$\langle T(\mathbf{k})^2 \rangle = \langle a_{lm}^2 \rangle \equiv C_{l(k)}, \quad (5)$$

in which the angular brackets stand for ensemble averaging, and the C_l give the angular power spectrum of the CMB. According to the ergodic hypothesis, the ensemble average is equivalent to the spatial average. Thus,

$$\langle a_{lm}^2 \rangle = \frac{1}{2l+1} \sum_{m=-l}^l a_{lm}^2, \quad (6)$$

which, as indicated in (5) is the square of the width of a Gaussian distribution, namely $T(\mathbf{k})$. The probability of a given $T(\mathbf{k})$ follows a Gaussian distribution just as the a_{lm} follow a Gaussian distribution.

The temperature map in Fourier space, $T(\mathbf{k})$, is arranged into a grid in which each grid point is assigned physical angular coordinate values k_x and k_y , which are related to the numerical k_{xn} and k_{yn} values (each ranging between 0 and $N_{max} - 1$) by

$$\begin{aligned} k_x &= \frac{2\pi}{L}(k_{xn} - k_{max}) \\ k_y &= \frac{2\pi}{L}(k_{yn} - k_{max}) \end{aligned} \quad (7)$$

in which the k_x and k_y values run from $-k_{max}$ to k_{max} . The value of k_{max} corresponds to the angular resolution of the data set. Note that this setup requires us to have an odd number of pixels in our Gaussian map. If an even number of pixels is required, the Gaussian map can be stripped of a row and column once it is constructed.

Using

$$\lambda = \frac{360^\circ}{l} = \frac{2\pi}{k}, \quad (8)$$

in which the wavelength, λ is measured in degrees and the wavenumber k is measured in inverse degrees, we compute the dependence of the degree of the spherical harmonic (mode number) $l(k)$ on the magnitude k of \mathbf{k} . Once this is done, we can look up the corresponding C_l for each \mathbf{k} from the output of a standard CMB simulation code (see below). Since $l(k)$ is not necessarily an integer, for each value of k , the program then determines the value $C_{l(k)}$ by linear interpolation between the C_l values of the two closest values of l corresponding to each $l(k)$.

Given the C_l values determined as described above, the Fourier space temperature map $T(k)$ can be determined by

$$T(k_x, k_y) = \sqrt{C_{l(k_x, k_y)}/2}(g_1(k_x, k_y) + ig_2(k_x, k_y)) \quad (9)$$

where $g_1(k_x, k_y)$ and $g_2(k_x, k_y)$ are randomly generated numbers obtained from a Gaussian distribution with variance one and mean of zero.

Since the position space temperature map $T(\mathbf{x})$ must be real, then $T(\mathbf{k})$ must satisfy $T(\mathbf{k}) = T^*(-\mathbf{k})$.

In summary, we derive $T(\mathbf{k})$ from the values of C_l determined as described above, and $T(-\mathbf{k})$ making use of the Hermitian property. Finally, to compute $T(\mathbf{x})$, we perform a Fast Fourier Transform on $T(\mathbf{k})$. Figure (2) shows the output of a temperature map with pure Gaussian noise.

We use the Code for Anisotropies in the Microwave Background (CAMB) [50] to generate the CMB temperature map generated by inflationary perturbations. CAMB, like the code on which it is based, CMBFAST [51], employs the line of sight integration prescription to compute CMB anisotropies. The advantage of using CAMB is that it computes C_l 's for higher l 's. Whereas CMBFAST can at best compute the power spectrum to $l = 3000$, corresponding to a resolution of 10 arcminutes, we use a power spectrum generated by CAMB up to $l = 22000$, corresponding to a resolution of 1.39 arcminutes. Simulations with higher resolution will enable us to place lower bounds on the string tension of cosmic strings. Additionally, high resolutions are necessary to apply our algorithm in the future high resolution CMB experiments such as ACBAR [52] and the South Pole Telescope [30].

The parameters we use for our simulations are standard Λ CDM concordance parameters based on fitting the model to a multi-experiment data set CMBall [53], namely $\Omega_b h^2 = 0.0227$, $\Omega_c h^2 = 0.112$, $\Omega_m = 0.26$,

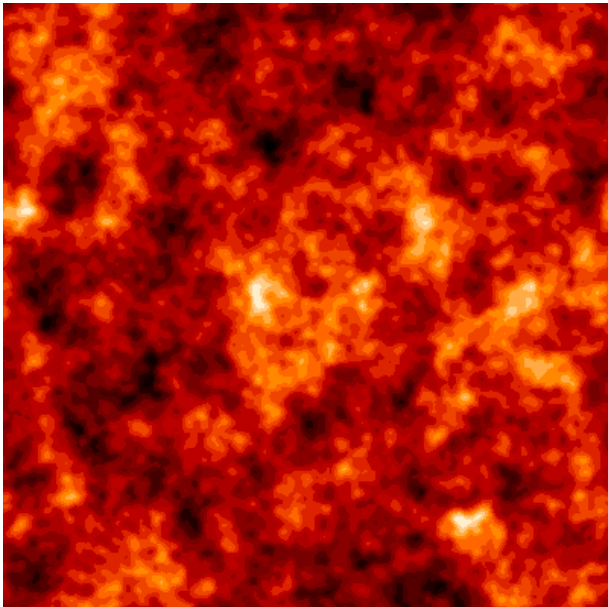


FIG. 2: Figure of the gaussian temperature map with a window of 10° and a resolution of 1.5 arcminutes.

$H_0 = 71.8$, $n_s = 0.965$, $w = -1$ (the equation of state for dark energy), $\Omega_\nu h^2 = 0$, $T_{CMB} = 2.726$ (the temperature of the CMB), $Y_{He} = 0.24$, and reionization optical depth, $\tau_{reion} = 0.093$.

B. Temperature Map from pure Cosmic Strings

Next we generate a temperature map of superimposed straight line segments representing the effects of long cosmic strings obeying the scaling solution. As in the Gaussian simulation, each grid point is assigned a temperature fluctuation $\Delta T/T$.

For simplicity we do not include the effects of string loops or of the small scale structure on the strings. According to the current status of cosmic string simulations, the effects of long strings dominate the cosmic string CMB sky. Small-scale structure on the long strings would maintain the KS effect (albeit with slightly reduced amplitude). Thus, in terms of searching for the KS signature of strings, the simplifications we use can be justified as a first step. Going beyond this approximation would require much more involved simulations (like those of [54]) with many more parameters.⁴ In future work we

plan to apply our Canny algorithm code to temperature maps obtained from more sophisticated simulations that include more detailed structure of cosmic strings.

In contrast to the Gaussian string map which is set up in Fourier space and transformed to position space via a Fourier transform, the string maps are set up directly in position space. As explained in the Introduction, each long string whose region of influence intersects the past light cone of the window in the sky we are considering will contribute a KS signal. We assume that the area in the sky affected by the temperature discontinuity of a single straight string segment per the KS effect is a rectangular box on each side of the string. The depth of the box (length perpendicular to the string) is equal to the Hubble length [28]. The size of the box in direction of the string is taken to be the product of the Hubble length and a length coefficient γ . The Hubble length corresponds to the time at which the past light cone intersects the region of influence of the string. We apply the KS signature by adding a positive temperature fluctuation to grid points in the box on one side of the string, and by adding the corresponding negative temperature fluctuation to the grid points in the box on the other side of the string.

We are using a toy model for the cosmic string distribution first introduced in [55] and also used by Pogosian et al. in [40]. It is based on a simple representation of the distribution of long strings as described by the scaling solution. According to this solution, the distribution of long strings is at all times like a random walk with a step length which is of the order of the Hubble radius at that time. We will denote this length by γH^{-1} , where γ is a constant factor of order one. Physically, this length represents the mean curvature radius of the string network. In the toy model, this distribution is approximated by a collection of straight string segments of length γH^{-1} .

One can argue that the curvature radius of the network of long strings must be of the order of the Hubble radius. If the curvature radius is larger than the Hubble radius, the strings will sit there as the universe expands until the Hubble radius catches up. If the curvature radius is less than the Hubble radius, then the strings will oscillate wildly, intersect and split off string loops (which then decay by gravitational radiation) until the curvature radius catches up to the Hubble radius. So the curvature radius will always be of order of the Hubble radius. The key ingredients in this argument are, firstly, that the effective action for a cosmic string is the Nambu-Goto action and hence the string dynamics is relativistic, and secondly that when strings cross they will intercommute, i.e. exchange ends, thus allowing the production of string loops.

Since the strings are relativistic, the distribution of strings will have changed after one Hubble time. Snap-

⁴ Although in principle cosmic string models are determined by a single parameter, namely μ , the cosmic string evolution cannot be followed either analytically or numerically without making additional assumptions, in particular on how cosmic strings interact. The results obtained in different numerical analyses concerning the string loop distribution vary by orders of magnitude (see e.g. the different results obtained in [15–17]), whereas the results for the distribution of long strings are comparable. Thus,

whereas limits based on long strings are robust, those which include effects of string loops are not.

shots of string distributions at time steps separated by Hubble time intervals will, when rescaled to the Hubble radius, look like independent realizations of a stochastic process. Hence, in our toy model of the distribution of long strings, we take the string segments to be independently distributed over time intervals greater than a Hubble time.

The input parameters for the string map generating function are the number of pixels on each side of the window, the number of degrees the window subtends, the number of strings per Hubble volume per the scaling solution, the string tension, $G\mu$, and the length coefficient γ .

The procedure to simulate cosmic strings is to follow the past light cone in time intervals $t_{n-1} \leq t < t_n$, where $t_{n+1} = \alpha_1 t_n$, from the time of last scattering to the present time. If $\alpha_1 = t_{n+1}/t_n = e$ then there are approximately 15 time intervals.

Next we project all strings present in one Hubble time interval to a fixed time hypersurface at the center of the time interval. This is done for all time intervals. On the microwave sky, the Hubble length in degrees corresponding to the comoving distance of the Hubble radius in space at the n 'th time interval can be shown to be (making use of the equation of state and of the Friedmann equation)

$$d_c(t_{n+1}) = d_c(t_n)\alpha_1^{1/3}, \quad (10)$$

in which $d_c(t)$ is in degrees. This recursion relation starts with $d_c(t_0) = 1.8$.

We need to find all of the strings which for a fixed time interval influence the CMB temperature map of the observed window. Instead of simulating only strings in the observed window, we must consider all strings in an extended window. This protects us from missing strings that start outside of the observed window but extend into it. At each time interval, the extended window is a square with each side subtending the degrees of the observed window added to twice the Hubble distance for that time step. The observed window is the central section with one Hubble length on either side.

Next we compute the number of Hubble volumes the extended window subtends at each time step, and the number of strings in each extended window. The number of Hubble volumes is obtained as the square of the number of degrees subtended by each extended window divided by the degrees subtended by each Hubble distance. The number of strings expected in the extended window for each time step is the rounded product of the strings per Hubble volume (determined as an input parameter based on the scaling solution) and the fraction/number of Hubble volumes a window subtends for each of the 15 time intervals.

Next we loop through each time step and each expected string in the extended window to determine where the string should be placed in the extended window and to place it by constructing a temperature differential. This is completed in a separate function in the program.

To simulate the strings, the program randomly places a line segment with a length given by $\gamma \cos \alpha H^{-1}$, where the Hubble length H^{-1} is in radians for the given time step. The angle α runs from 0 to $\pi/2$. Multiplying by $\cos \alpha$ accounts for a projection from three to two dimensions. Although technically the length of the string should be multiplied by a coefficient given by projecting a geodesic on a sphere onto a plane, since we are dealing with small window sizes and the flat sky approximation is appropriate, this complication is unnecessary. The location of the beginning of the string and its direction are determined randomly. The location of the beginning of the string is given by taking the product of a random number between 0 and 1 for both directions on the grid and the length of the extended window in radians. The direction of the placement of the string, i.e. the angle θ of the string, is chosen by a randomly generated number between $-\pi/2$ and $\pi/2$. This is the direction of the string as given by the angle from the x-axis. Finally, a binary flag is used to determine which side of the string will be a positive temperature fluctuation and which side will be a negative temperature fluctuation. The value of the flag is randomly determined.

Next the code computes (from the location of the start of the string and the direction of the string) the end point of the string and each corner of the box around each side of the string and each slope for each boundary of the box.

The routine loops over each pixel in the observed window, starting in the lower left hand corner, to determine if the pixel lies within the box affected by the cosmic string. If it does, the temperature is changed by δT . The sign of δT is determined by the temperature flag delineated above. The temperature fluctuation is given by

$$\frac{\delta T}{T} = \tilde{v} r 4\pi G\mu \quad (11)$$

in which $T = 2.726$ is the background CMB temperature. In the above, \tilde{v} represents the root mean square (over all strings) value of $v\gamma(v)$, where v is the transverse velocity of the string and its relativistic γ factor is $\gamma(v)$. Also, r a random number between 0 and 1 which adjusts the velocity to take into consideration the different velocities that the string might have as well as the projection of the velocity of the string onto the plane perpendicular to the line of sight. Based on recent cosmic string evolution simulations we use the value $\tilde{v} = 0.15$.

Figure 3 shows the temperature map produced by a simulation with a few test cosmic strings (not a scaling solution). The temperature boxes produced by the individual strings are clearly visible. Figure 4 demonstrates the corresponding results from a full string simulation with $N = 1$, i.e. one string per Hubble volume. The straight line temperature discontinuities produced by individual strings are still visible. However, there are a lot of overlap regions since a given photon will during its trajectory pass close to several strings. The overlapping problem gets worse for $N = 10$, as clearly visible in Figure 5.

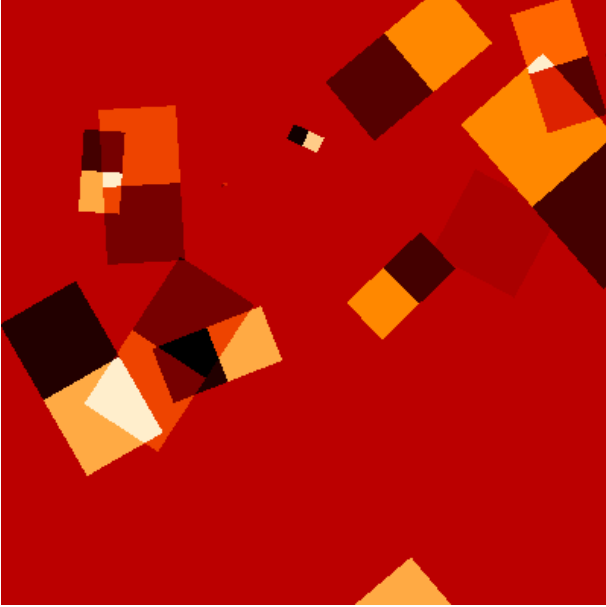


FIG. 3: A cosmic string simulation for a few strings. The light areas represent where the temperature fluctuation is positive and the dark areas represent where the temperature fluctuation is negative.

As a further test of the algorithm described in this subsection we show the resulting angular power spectrum of temperature anisotropies. The figure (Figure 6) is for a pure cosmic string map with $N = 10$ and $G\mu = 6 \times 10^{-8}$. The range of l values are limited from below by the angular size of the simulation box, and from above by the angular resolution we have chosen. The error bars are standard errors of the mean based on 100 runs. As theory predicts [25, 57], the angular power spectrum is approximately scale-invariant on large angular scales (the deviation from scale-invariance at the lowest values of l is presumably a boundary effect), and its amplitude is consistent with what is expected.

C. Sum of Gaussian Map and Cosmic String Map

Our goal is to test if the Canny algorithm is able to pick out the KS signature from strings even if the strings are a subdominant component to the CMB fluctuations. To test this, we need to produce temperature maps which contain both cosmic strings for some value of $G\mu$ and a spectrum of Gaussian fluctuations like in the concordance Λ CDM model, except with an amplitude of the Gaussian noise which is reduced such that the total angular CMB power spectrum remains consistent with either simulations or observations.

Here we describe how to find the coefficient, a , for each map which will be used to add the pure string map to the pure Gaussian map to get a Gaussian map with

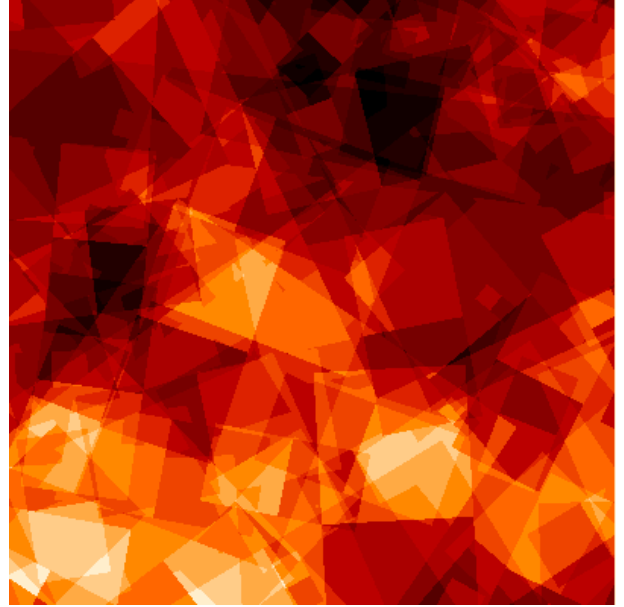


FIG. 4: The CMB temperature anisotropy map produced by a scaling cosmic string simulation with $N = 1$. The discontinuity lines in the maps produced by the KS effect are clearly visible, but there are a lot of overlap regions where a number of strings affect the temperature at a fixed point.

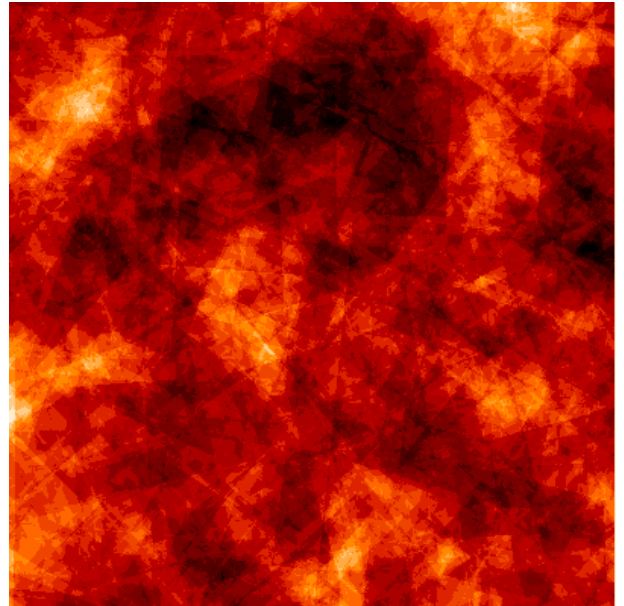


FIG. 5: The CMB temperature anisotropy map produced by a scaling cosmic string simulation with $N = 10$. In this case the effects of overlaps is much more pronounced.

superimposed strings,

$$T_{G+S}(\mathbf{k}) = aT_G(\mathbf{k}) + T_S(\mathbf{k}), \quad (12)$$

with T_{G+S} as the temperature of the Gaussian map plus pure string map and T_G and T_S as the temperature maps of the concordance Gaussian and string simulations re-

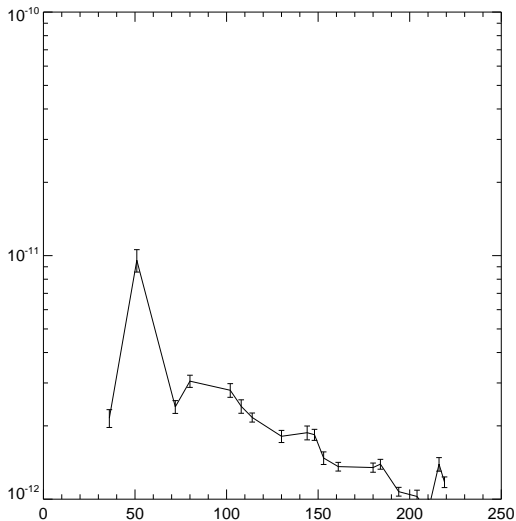


FIG. 6: The angular power spectrum of the CMB anisotropy maps of pure cosmic string simulations with values $N = 10$ and $G\mu = 6 \times 10^{-8}$. The horizontal axis is l , the vertical axis is $l(l+1)C_l$.

spectively. Alternatively, we could use the temperature map of the best current data, the five year results of WMAP [58], for T_G . It is important to use consistently either the temperature map from experimental data or from theoretical simulations for both T_G and T_{G+S} since the C_l 's for the two models are not identical.

We want the model to give the best possible agreement with the data, either experimental or simulated. Hence, the plan is to adjust the coefficient a so that the combined string and Gaussian map, $T_{G+S}(\mathbf{k})$, fits the data best. This means that we adjust the Gaussian map so that the corresponding C_l 's of $T_{G+S}(\mathbf{k})$ give an optimal fit to the data. Since the error bars on the observed angular power spectrum C_l are smallest relative to the signal in the range from $l_{min} = 10$ to $l_{max} = 220$ we shall fit the C_l 's within this range. Note that this range includes most of the first Doppler peak region. Now for values of l comparable or larger than that corresponding to the first Doppler peak, the contribution from strings is dominated not by the Kaiser-Stebbins effect from strings between t_{rec} and t_0 , but from string-induced fluctuations at last scattering which are not included in our analysis. Thus, there is an intrinsic inaccuracy in the determination of the value of a . If we were to take l_{max} to be the value where the Kaiser-Stebbins effect ceases to be dominant (a value much smaller than 220), then we would obtain a smaller value for a and hence a better discriminatory power of our algorithm. However, this procedure would be worse than the one we have adopted, since we would be working with a power spectrum which is a much worse fit to the observations in the Doppler peak region than the one we are using. Our choice of l_{max} can thus be considered to be a conservative one.

The first step is to find the C_l values from the pure string map. To do this, the routine initially takes the inverse FFT of the temperature fluctuation $T(\mathbf{x})$ to compute $T(\mathbf{k})$. Then, using $k = 2\pi l/360$, the routine computes the wave number magnitudes $k(l)$ for all values of l in the our range. Then the value of δk corresponding to $\delta l = 1/2$ is found.

Next, the map summation routine finds the wavenumber magnitude k for all values of \mathbf{k} (whose components range from $-k_{max}$ to k_{max}). For each value of l in the range between l_{min} and l_{max} the code finds the components k_x and k_y of all waves for which the magnitude of k lies within δk of $k(l)$. Knowing k_{xn} and k_{yn} we can find the corresponding $T(\mathbf{k})^2$ for each of the wavenumbers. Once all of the $T(\mathbf{k})^2$ values are found for each l , we find the average to get $\langle T(\mathbf{k})^2 \rangle$ for each l . These values are the C_l values of the pure cosmic string map for all l between l_{min} and l_{max} .

Since

$$T_{G+S}(\mathbf{k}) = aT_G(\mathbf{k}) + T_S(\mathbf{k}) \quad (13)$$

we obtain

$$\langle T_{G+S}(\mathbf{k})^2 \rangle = a^2 \langle T_G(\mathbf{k})^2 \rangle + \langle T_S(\mathbf{k})^2 \rangle + 2a \langle T_G(\mathbf{k})T_S(\mathbf{k}) \rangle. \quad (14)$$

However, $\langle T_G(\mathbf{k})T_S(\mathbf{k}) \rangle = 0$ because the Gaussian and string temperature fluctuations are independent. Hence

$$C_{l(G+S)} = a^2 C_{l(G)} + C_{l(S)}. \quad (15)$$

Now that we have the C_l values for the simulated CAMB data, $C_{l(G+S)}$, the C_l 's we found for the pure cosmic string map, $C_{l(S)}$, and the C_l 's for the simulated gaussian map from CAMB, $C_{l(G)}$, we can compute a^2 for each l by viewing (15) as a defining relation for a^2 . Obviously, for each value of l we will get a different answer. To compute a single coefficient a which best fits all of the l 's from l_{min} to l_{max} we perform a linear fit on the coefficients, a , for each l . We use the best fit y -intercept of a linear model fit by minimizing the χ^2 error statistic for a . The y -intercept can be used because the slope of the best fit to the linear model is negligible.

Once a is found for a particular string image, the result is averaged over all of the generated simulated string images to obtain the final value for a which is then used for all the string maps of a given $G\mu$.

Figure (7) shows the resulting CMB anisotropy map in a simulation with a large value of $G\mu$ chosen such that the strings play an important role. Comparing the map to the pure string map of Figure (5) we see that the string-induced line discontinuities are still visible. However, in the case of a lower value of $G\mu$ the effects of the strings are not visible by eye and we need to resort to a statistical analysis to study whether the map is distinguishable from that of pure Gaussian noise (Figure (8)).

We use the algorithms described in this section to generate maps with and without cosmic string signals. The main question we would like to address now is down to

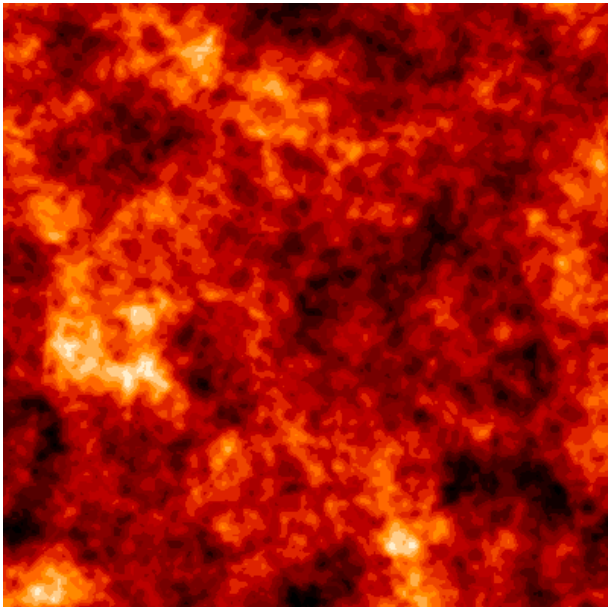


FIG. 7: The smoothed CMB temperature anisotropy map produced by a simulation with both Gaussian noise and cosmic strings with $G\mu = 3.5 \times 10^{-7}$ and $N = 10$. In this case the KS discontinuity lines are visible.

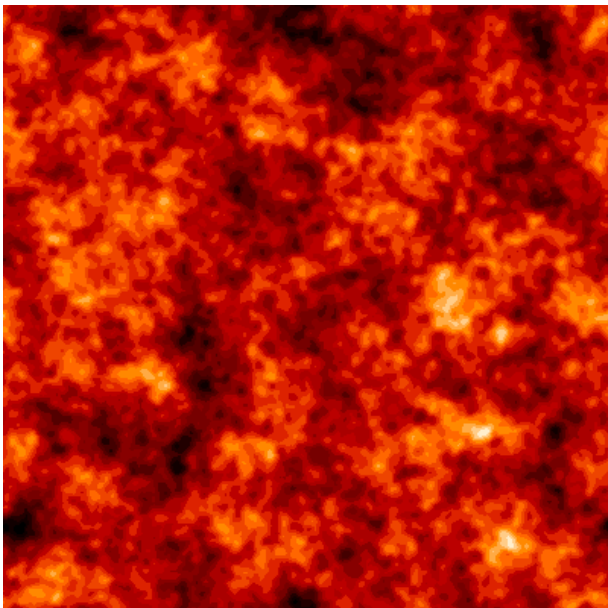


FIG. 8: The CMB temperature anisotropy map produced by a simulation with both Gaussian noise and cosmic strings with a smaller value of $G\mu$, namely $G\mu = 2 \times 10^{-8}$ and $N = 10$. In this case the KS lines are not visible by eye.

what value of $G\mu$ the Canny edge detection algorithm is capable of distinguishing between these two sets of maps in a statistically significant way. In the following section we describe our realization of the Canny algorithm routine which turns a microwave temperature map into an edge map, the edges standing for lines across which the

gradient is a local maximum.⁵

III. IMPLEMENTATION OF THE CANNY ALGORITHM

In this section we describe our implementation of the Canny algorithm. In its original version [47], the Canny algorithm is intended to find lines in the map with maximal gradients across the line. In this way, the algorithm can be applied to the image of a face and returns a map where only the pixels of the map with the strongest features are shaded in. Similarly, the algorithm could be applied to find crystal defect lines on metallic surfaces. Our original work applying the Canny algorithm to CMB maps [46] also was based on this idea.

However, to look for cosmic strings we are less interested in the local maxima of the gradient map which overall have maximal amplitude. Rather, we are interested in local maxima of the gradient for which the amplitude of the gradient is in correspondence to the expected KS signal. Thus, in contrast to the original Canny routine which uses two thresholds, we here introduce a modified algorithm in which three gradient thresholds are made use of (as in [48]). The use of the thresholds is described below.

We will first give a brief overview of how the algorithm works. First, an optional part of the Canny algorithm is to smooth the map in order to eliminate shot noise. The second step in the algorithm is to construct a map of the temperature gradients. Next, locations must be identified which correspond to local maxima of the gradients. The maximal average gradient of the pure string map determines the three thresholds used. The fourth part of the algorithm involves selecting among the grid points identified as local maxima those which have the right range of magnitudes. Gradients larger than some upper threshold are not due to single strings and will hence be discarded. Those above a second threshold quite close to the expected edge strength will be kept. To take into account the fact that Gaussian noise may well decrease the amplitude of some pixel along a string edge below the above-mentioned threshold, we introduce a third (the lowest) threshold and keep the pixels whose gradient is larger than that threshold, provided that the pixel is connected to a pixel with gradient amplitude above the second threshold (and provided that the gradient directions are appropriate and that the pixel is connected to a pixel in one of the allowed directions relative to the gradient). The pixels thus selected form the Canny edge map. Given the pixel edge map, a next step in the algorithm is to identify the edges in the pixel edge map.

⁵ In our realization of the algorithm, we impose an additional requirement, namely that the gradient magnitude is tailored appropriately to the expected cosmic string signal.

The length of each edge is found, and a histogram of edge lengths is produced. The analysis part of the algorithm then checks if for a fixed value of $G\mu$ the histograms of a pure Gaussian noise map and of a noise map including a contribution of cosmic strings (and appropriately reduced amplitude of the Gaussian noise) are statistically significantly different.

In implementing the Canny algorithm, several (three) choices must be made beyond fixing the three thresholds used. We look for the set of choices which give the best differentiation between maps with and without strings.

The first step in our implementation of the Canny algorithm is the filtering of the data. This filtering is intended to eliminate point source noise. In studies like the present one in which we are dealing with simulated data which has no noise, the maps can be used without smoothing. In order to eliminate point sources, smoothing should be used in the case of real data. We have explored the effects which smoothing has.

The routine first produces an un-normalized filter map $\tilde{F}(i, j)$ (i and j are integer labels running from 1 to N_f indexing the pixels of the filter map)

$$\tilde{F}(i, j) = e^{-\frac{x^2+y^2}{2\sigma^2}} \quad (16)$$

in which $x = i - (N_f - 1)/2$, $y = j - (N_f - 1)/2$, $\sigma = 0.5N_f$, and N_f is the number of pixels along one direction of the filter map, an input parameter in the smoothing routine. The normalization is the sum of all of the unnormalized weights

$$C_1 = \frac{1}{\sum_{i,j} \tilde{F}(i, j)}. \quad (17)$$

Now we can determine the normalized filter map as

$$F(i, j) = C_1 \tilde{F}(i, j). \quad (18)$$

Finally, we convolve the input temperature map with the filter map to obtain the filtered data map. If $M(i, j)$ denotes the initial map, then the filtered map $FM(i, j)$ is given by

$$FM(i, j) = \sum_{k,l=1}^{N_f} M(i-x, j-y)F(k, l), \quad (19)$$

where x and y are determined from k and l as indicated below (16). Boundary points require special treatment. We repeat the points at the boundary.

The second part of the algorithm involves constructing the gradient maps. Two arrays are created, the first containing the magnitude of the gradient at each pixel of the map, the second containing the information about the direction of the gradient.

We compute the lattice derivatives by shifting the temperature map in each of the eight directions and looking for the maximal difference. Instead of using the usual

lattice gradient which is defined by

$$\hat{G}(x, y) = \frac{G(x + \epsilon, y) - G(x - \epsilon, y)}{2\epsilon} \hat{x} + \frac{G(x, y + \epsilon) - G(x, y - \epsilon)}{2\epsilon} \hat{y}, \quad (20)$$

(where the grid spacing is ϵ), we shall use the following as our definition of the magnitude of the gradient:

$$G(x, y) = \max|\Delta G| \quad (21)$$

and the direction is taken to be that for which the maximum value of $|\Delta G|$ occurs. ΔG is given by the discrete gradient

$$\Delta G(x, y) = \frac{G(n(x, y)) - G(x, y)}{d(x, y)}, \quad (22)$$

where $n(x, y)$ denotes the neighboring point to (x, y) and $d(x, y)$ is the distance between $n(x, y)$ and (x, y) . For neighboring points not on the diagonal, the distance between the neighboring point and the point (x, y) is 1, for points along the diagonal the distance is $\sqrt{2}$.

The gradient of the image is then stored as an array with a dimension containing the two dimensional pixel array with the edge strengths and a dimension containing the two dimensional pixel array with the edge directions as the values.

The next step is to find the pixels of the map which correspond to local maxima in the direction of the gradient. We first shift the map one unit forwards and backwards in each of the four directions (along the coordinate axes and along the two diagonals, respectively). For each of these four shiftings we focus on points for which the absolute value of the gradient is greater than at the two neighboring points on either side. For all points selected, we check if the gradient is in the direction of the shifting. Pixel points which pass this test are kept. The others are assigned a value of 0. Boundary pixels are stripped from the list of local maxima since their magnitudes are influenced by boundary effects. In Appendix A we discuss the local maxima doubling problem which the code has to deal with.

As mentioned at the beginning of this section, our implementation of the Canny algorithm makes use of three thresholds t_u , t_l and t_c . Their values are chosen to correspond to the amplitude of the KS effect of a single string since it is this effect which we want to identify.

Thus, to set the thresholds for a given value of $G\mu$, we first run the code on a number of pure string simulations for that value of $G\mu$. We determine the maximal gradient (amplitude) $G_{max,i}$ for each simulation, and define the ‘‘string maximal gradient’’ G_m as the average of the individual maxima $G_{max,i}$.

Returning to our list of candidate local maxima, then if the amplitude is larger than $t_c G_m$ the point is discarded since it is not due to a typical string gradient. For amplitudes in the range

$$t_u G_m < \mathcal{A} \leq t_c G_m \quad (23)$$

then the pixel coordinates and gradient directions are stored in arrays. Later on, the edge pixel map will be constructed by marking all pixel points in the above-mentioned coordinate array as 1. These are pixels for which the gradient is in the right range to be due to the KS effect from a cosmic string. Pixels with a slightly lower gradient amplitude might still be due to the KS effect from a string with amplitude slightly reduced by noise. It is advantageous for the success of the Canny algorithm to take into account this possibility. Thus, if the amplitude of the local maxima is in the range

$$t_l G_m < \mathcal{A} \leq t_u G_m \quad (24)$$

then the coordinates and gradient directions of such pixels are stored in arrays corresponding to pixel points marked 1/2. Arrays are created to store the indices of the points marked as 1 and 1/2 and separate arrays are created to store the directions of the corresponding indices.

The next step is the “edgefinder” routine which decides whether grid points marked as 1/2 belong to an edge or not. Roughly speaking, points marked as 1/2 are considered as belonging to an edge if they are direct or indirect neighbors to points labelled by 1 and the gradients are in a similar direction. To specify the routine, there are three choices which can be made for this algorithm, as will emerge below. We start from a point labelled 1 (an option in the program is to start with a point labelled 1/2 - the first of the three choices mentioned above)⁶. The program then searches in all eight directions for a contiguous point labeled as 1/2 or 1. For each direction, we check if it lies in the six directions (or 2 directions) perpendicular or near perpendicular (or just perpendicular - the second of the choices mentioned above) to the original point’s gradient and check if the gradient is in the appropriate parallel or near parallel (or just parallel - the third choice) direction to that at the original 1 (or 1/2). If a point labeled as 1/2 is found, and the direction is in one of the allowed six (or two), then we mark the coordinates of that point and repeat the search starting from that point. We stop if a 1 is found, in which case we convert all of the 1/2s found on the way to 1. If we do not find another point labelled 1/2, we stop and do not change the labelling of the points encountered on the way. Then, we move on to the next point labelled by 1 which has not already been covered by the search. In the variant of the code in which the search starts with points labelled by 1/2, we search for points labelled by 1/2 or 1 as described above, mark the coordinates of the points found, and continue until either a point marked 1 is found (in which case all of the 1/2 found are converted to 1), or else no new point is found, in which case the

1/2 are considered not to belong to a common edge and are not relabelled.

The output of the “edge-finder” routine is a list of coordinates of the pixels marked by 1 and of the corresponding gradient directions. The result of the algorithm can be represented by two maps. The first is a map of pixel points originally labelled as 1 and 1/2 (different shades), the second is an initial “edge pixel map”, the map of the set of pixels labelled at the end of the “edgefinder” routine by a 1.

The final part of the Canny algorithm is an “edge-counting” routine (this part of our method goes beyond the standard Canny algorithm). This routine creates a second “edge pixel map” and a histogram of number of edges as a function of the edge length. Starting with the first entry in the list of pixels marked by 1, the routine searches in directions perpendicular or near perpendicular (or exactly perpendicular only) to the gradient direction to find other pixels labelled as 1. If such a pixel is found, then the routine checks if the gradient direction of the new pixel is near parallel or parallel (or exactly parallel only) to the direction of the gradient at the initial pixel. If this is the case, the routine considers the new pixel as part of the edge it is following. Once no further pixel is found, the routine considers the edge to have ended and saves the result. The program then moves to the next pixel labelled by 1. Pixels are only allowed to be counted in one edge. After all edges are found, the lengths are tallied and can be made into a histogram. To take into account the fact that a pixel may be missing from a string edge due to a large influence of the Gaussian component, there is an option for the “edge-counting” routine to allow for a gap in an edge of a certain length. This skipping length parameter is a further input parameter which the user of the algorithm has to set. As should also be obvious from the discussion in this paragraph, the same choices of “perpendicular exactly or nearly perpendicular” or “perpendicular exactly” and “parallel exactly or nearly parallel” or “exactly parallel” as in the “edge-finding” routine are open to the user in this part of the program.

Let us conclude this section by reminding the reader of the various parameters which have to be chosen and choices which have to be made in our Canny algorithm implementation. First of all, in our “edgefinder” routine there are the three thresholds t_c , t_u and t_l which are used in the labelling of the local maxima. Next, in our routine to turn 1/2 pixels into 1 pixels, there are three choices to be made, first whether one starts with 1 or 1/2 pixels, second whether one searches for neighboring 1s and 1/2s in direction perpendicular or in directions nearly perpendicular or perpendicular to the direction of the gradient, and third whether one demands that at the selected neighboring site the gradient is parallel or if it is nearly parallel or parallel to the direction of the gradient at the initial point. In the edge counting algorithm there are the two choices analogous to the two choices mentioned at the end of the previous discussion. The user of

⁶ Note that the algorithms starting from 1 or 1/2 are in fact different. This is also noted in footnote 7.

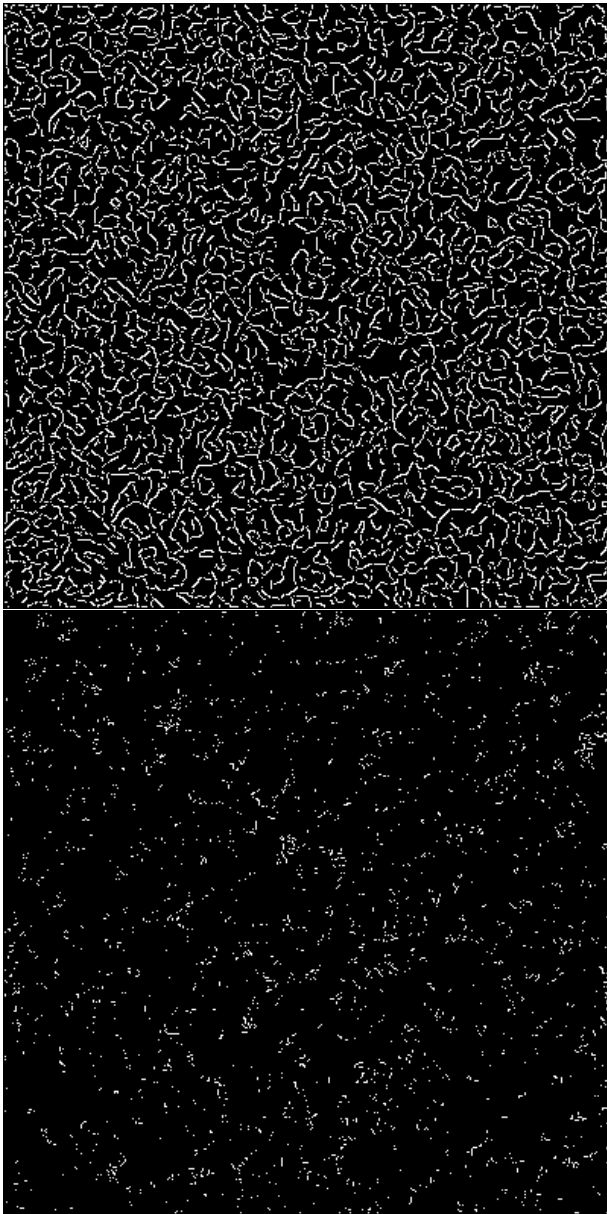


FIG. 9: Edge maps for the gaussian map shown before. The first edge map is for a G_m and thresholds used in the analysis of an $N = 10$ gaussian map with strings for $G\mu = 3.5 \times 10^{-7}$. The thresholds are $t_c = 2$, $t_u = 0.25$, $t_l = 0.1$. The second edge map is made for the same gaussian map used in the analysis of an $N = 10$ gaussian map with strings for $G\mu = 2 \times 10^{-8}$. The thresholds are $t_c = 4$, $t_u = 0.25$, $t_l = 0.1$.

the program has similar choices of “perpendicular exactly or nearly perpendicular” versus “perpendicular exactly” to the gradient for the directions to search and “parallel exactly or nearly parallel” versus “parallel exactly” to make. Finally, there is the number of points which the “edge-counting” routine can skip.

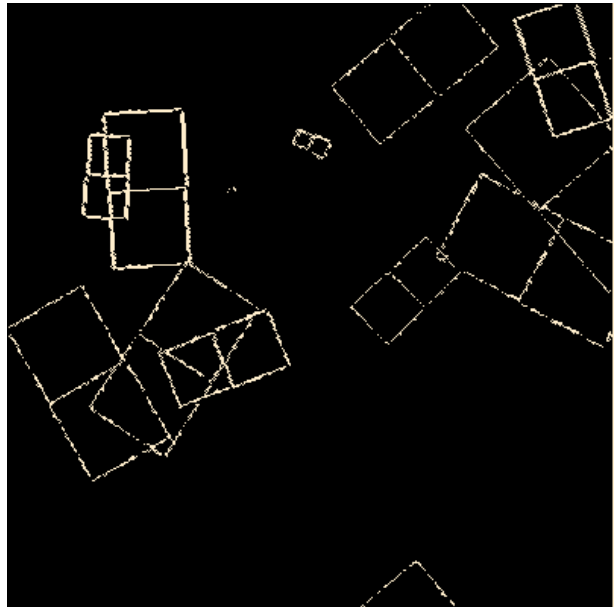


FIG. 10: The test string edge map.

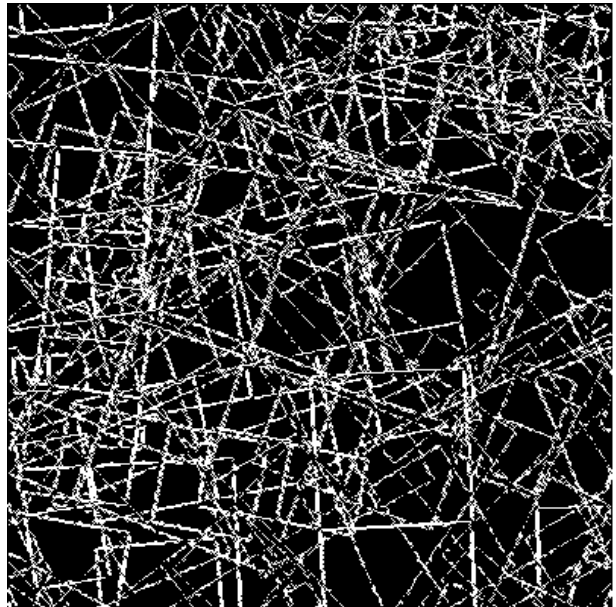


FIG. 11: N=1 pure string edge map.

IV. ANALYSIS

We tested the capability of our implementation of the Canny algorithm to distinguish between temperature anisotropy maps which arise from a pure Gaussian Λ CDM model and a model in which there is a contribution to the power spectrum coming from a scaling distribution of cosmic strings (and with the power of the Gaussian noise reduced to maintain the optimal fit to the CMB angular anisotropy power spectrum as described in Section II).

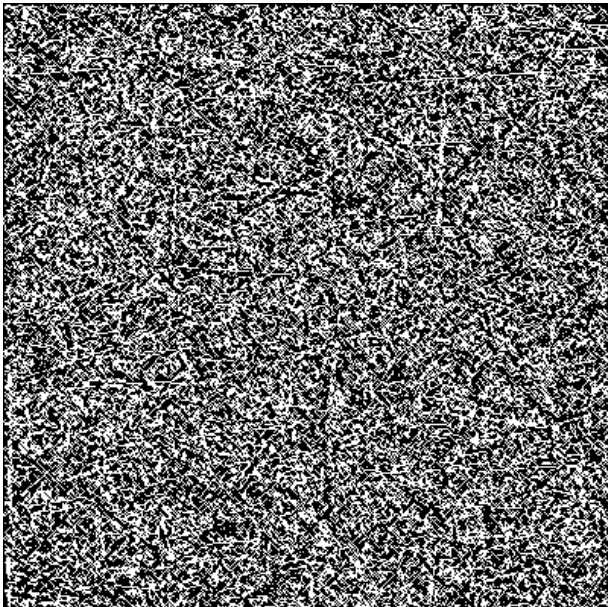


FIG. 12: N=10 pure string edge map.

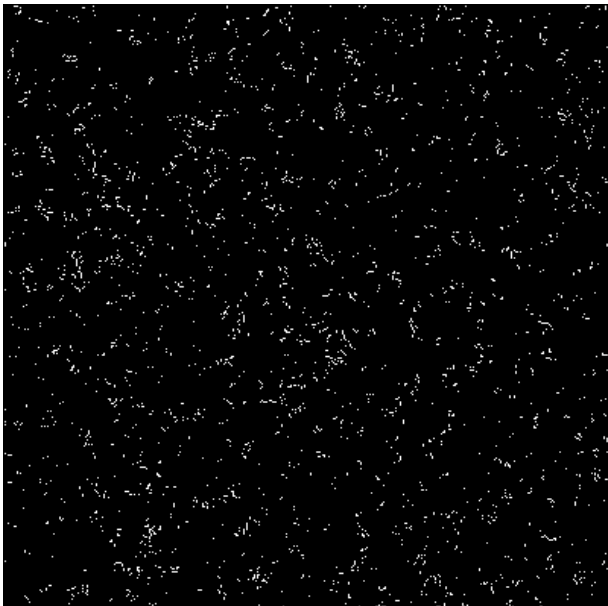


FIG. 13: $G\mu = 2 \times 10^{-8}$ unsmoothed string plus gaussian noise edge map. N=10. The thresholds are $t_c = 4$, $t_u = 0.25$, $t_l = 0.1$.

Since we have applications to small-scale CMB anisotropy experiments in mind, we choose a simulation box of edge length 10° and with angular resolution of $1.5'$. Both in the Λ CDM model and in the cosmic string model, the actual universe is a realization of a random process. Thus, in order to determine whether the Canny algorithm can distinguish between the predictions of the two theories, we have to run many realizations of the models. We ran 50 simulations for both theories. This number was chosen since it is the number for which the

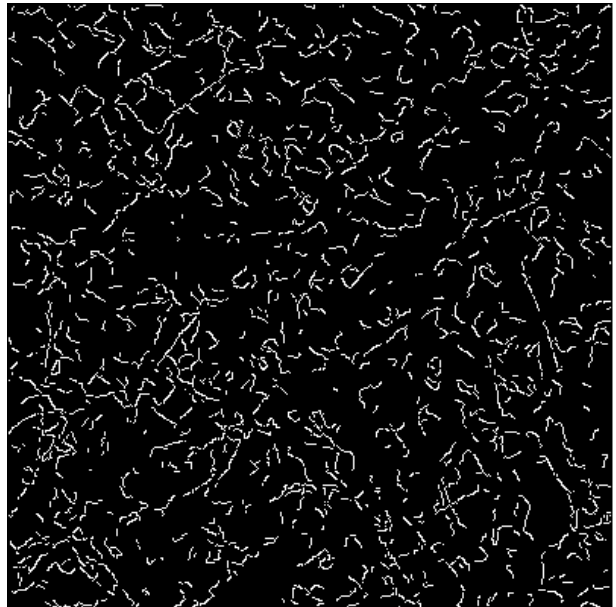


FIG. 14: $G\mu = 3.5 \times 10^{-7}$ smoothed string plus gaussian noise edge map. N=10. The thresholds are $t_c = 2$, $t_u = 0.25$, $t_l = 0.1$.

resulting probabilities converge.

For small values of $G\mu$, we generated each cosmic string map independently. For larger values of $G\mu$ we generated the temperature maps by rescaling the temperature map for $G\mu = 6 \times 10^{-8}$. The value of G_m was scaled accordingly. The value of the scaling factor a was computed for each of the simulations for fixed value of $G\mu$ independently. Because of large fluctuations in the various random variables (e.g. the number of strings), there results a spread for the values of a , and some of the values of a^2 were negative for large values of $G\mu$. Thus, for large values of $G\mu$ we used a common value for a^2 , namely the mean of the values of a^2 for $G\mu = 6 \times 10^{-8}$ and scaled according to (see [48]):

$$a^2 = 1 - \frac{\langle C_l^S \rangle_0}{\langle C_l^G \rangle_0} \left(\frac{G\mu}{G\mu_0} \right)^2 = 1 + (a_0^2 - 1) \left(\frac{G\mu}{G\mu_0} \right)^2$$

$$a_0^2 = 1 - \frac{\langle C_l^S \rangle_0}{\langle C_l^G \rangle_0}, \quad (26)$$

where the subscript 0 indicates the reference value of $G\mu$.

Both the models and the Canny algorithm contain a number of parameters. As described in Section II, we chose the best fit parameters of a Λ CDM model. For the cosmic string distribution, we considered $G\mu$ to be the free parameter of interest. We fixed the number of strings per Hubble volume to be $N = 1$ in some simulations and $N = 10$ in other simulations, the string segment length to be γH^{-1} with $\gamma = 1$, and the velocity parameter $\tilde{v} = 0.15$.

In this work we did a rough optimization of the various parameters which have to be chosen in the Canny algorithm. For a fixed value of $G\mu$ for which the effect

of the strings is statistically significant we varied the parameters to find the parameter values which gave the best discriminatory power (see below). On this basis, we chose the various thresholds. Concerning the optimization of the “flags” in the routine, it proved advantageous to start with the pixels marked 1 in the edge finding algorithm, and to look in directions both perpendicular and near to perpendicular, and allowing the gradient at the neighboring point to be parallel or near to parallel in both the edge finding and the edge counting routines ⁷.

We ran simulations both with and without smoothing of the maps. In the runs with smoothing, the smoothing was done in the final maps (after adding the string maps to the Gaussian maps). Finally, we ran simulations allowing for skipping of points in the edge counting algorithm.

Discriminating power was quantified using the *Fisher combined probability test*. This test is applied to the two output histograms of edge lengths, one from the pure Gaussian simulations, the other from the strings plus Gaussian maps. For each length l , we are given the mean number of edges of that length and the corresponding standard deviation. Given the two means and corresponding standard deviations we can apply the t-test to compute the probability p_l that the two means come from the same distribution. The Fisher combined probability method then computes a χ^2 as follows

$$\chi_{2k}^2 = -2 \sum_{l=1}^k \ln(p_l) \quad (27)$$

where k is the number of edge lengths being considered, and computes the corresponding probability value from a χ^2 distribution with $2k$ values. We chose k to be the last edgelenhth to have a nonzero standard deviation in either the string or gaussian distributions, whichever is smaller.

The Canny routine makes use of three thresholds. To find the cutoff or top threshold we ran a script to find the maximum average gradient of the fifty string maps and then compared the highest gradient to the highest average gradient. This threshold needs to increase as the

⁷ We ran the Canny algorithm on two different test maps to develop an intuition on how to optimize the flags. For both test maps, more edges were found when the number of allowed directions and gradients were greater. In one test map more edges were found when the algorithm started with points marked as 1/2 and in the other algorithm more edges were found when the algorithm started with points marked as 1 for some values of the flags. Since the algorithm is much slower when it starts with points marked as 1/2, in this paper we always start with points marked as 1. Longer edges were found when skipping points was allowed. This is consistent with the findings we have for the averages of the full 50 maps of gaussian temperatures and the combined maps with strings. Since skipping reduces the number of short edges, where the standard deviation is smaller compared to the mean, and thus increases the p-value, it increases the probability that the maps look the same.

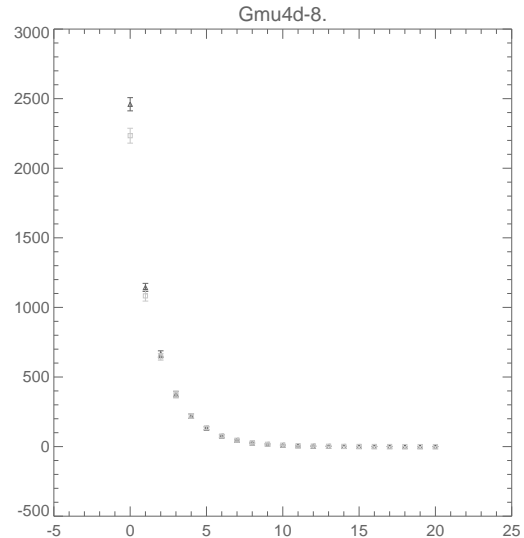


FIG. 15: Histogram of the edge length distribution of the unsmoothed pure Gaussian maps and the strings plus smoothed Gaussian maps for a value of $G\mu = 4 \times 10^{-8}$. The number of edgelenhths for strings plus gaussian maps are denoted by triangles and the squares denote the number of edgelenhths for the pure gaussian maps. We plot the means and the standard deviation as the error. Note the systematically larger number of edges for maps with strings for short edgelenhths.

$G\mu$ decreases because otherwise one throws out virtually all of the edges, since as $G\mu$ decreases G_m decreases. One needs to keep some edges with values greater than the maximum gradient in any string map because the signal from the gaussian map may add in the same location to the signal from the string map. To find the upper and lower thresholds we ran the Canny algorithm for various thresholds on a pure string map and determined by eye if enough strings could be seen but not so many that the overlap of the edges breaks apart the long string edges. In particular, for $N = 10$ if the thresholds are too small the images are saturated with short edges which break up the long edges. Thus, the thresholds need to be higher for $N = 10$ than for $N = 1$. We leave a detailed optimization of the thresholds to future work.

As a test of the code, we ran the analysis algorithm on two independent sets of fifty Gaussian CMB maps and computed the probability that the two sets come from the same Gaussian ensemble. The resulting probability was typically of the order of 0.7, i.e. within the 1σ error range.

Our simulations show that maps originating from cosmic strings have a larger number of edges than the corresponding pure Gaussian maps. This is a consequence of the presence of the Kaiser-Stebbins edges, the signal we are looking for. Figure 15 shows a comparison of the two histograms for the value $G\mu = 4 \times 10^{-8}$. Since the Gaussian noise cuts up the long edges, the difference in edge lengths is statistically significant only for short edges.

Table 1 summarizes our results obtained by applying the Fisher combined probability method to the histograms of string edge lengths. The results are for $N = 10$ (10 strings per Hubble volume per Hubble time), for un-smoothed maps, without skipping in the edge drawing and edge counting routines. The statistical analysis includes edgelenlength 1 data. The first column gives the value of $G\mu$, the second the value of the top threshold (the other two thresholds are held fixed at the values $t_u = 0.25$ and $t_l = 0.1$), the third gives the probability that the histograms of the string and Gaussian maps come from the same Gaussian distribution. The fourth value gives the maximal edge length used in the analysis, and the last column lists the value of a . We see that the cosmic string signal can be detected⁸ at a three sigma level down to a value $G\mu = 2 \times 10^{-8}$ which is almost two orders of magnitude better than the current bounds obtained by direct searches, and one order of magnitude better than the limits on $G\mu$ coming from the CMB angular power spectrum constraints. These results are for unsmoothed maps.

As can be expected from looking at the histograms of 15, the sensitivity of the algorithm decreases slightly if edges of length 1 are excluded from the analysis. The results excluding edges of length 1 are shown in Table 2.

Since smoothing dramatically reduces the number of short edges, and since the strength of the signal of our analysis comes from the number of short edges, it turns out that smoothing significantly weakens the ability of the algorithm to pick out strings. The results of our⁸ More conservatively, we should say that the difference between the maps with cosmic strings and pure Gaussian maps can be

analysis applied to smoothed maps (smoothing length 3) are given in Table 3. The loss in discriminatory power is about a factor of 5. This is a serious concern when considering applications of our algorithm to real data.

In Table 4 we present the results for $N = 1$. Since there are an order of magnitude less string edges in this case, the limit on $G\mu$ which can be obtained is slightly weaker (about a factor of 3 weaker). To put this result into context, it is important to point out that limits on $G\mu$ from other studies implicitly or explicitly use $N = 10$. The limits on $G\mu$ from matching the angular CMB power spectrum would be weaker by about one order of magnitude.

The results of the previous tables were obtained from an algorithm which did not have any skipping in the edge counting routine. We allowed skipping of two points. Skipping of two points leads to a larger number of long edges. Skipping by four points leads to edge broadening, an unwanted feature. Hence, we only considered skipping two points. Including skipping turns out to reduce the number of short edges more significantly than it increases the number of longer edges. Thus, the power of our routine to discriminate between maps with and without strings slightly decreases when introducing skipping (which is the opposite of what we initially expected). The results are indicated in the following table. However, it is possible that further optimization of the routine parameters would reverse the results concerning the effectiveness of skipping.

detected.

Table 1: Unsmoothed String Map versus Gaussian Map N=10
Minimum Edge Length: 1
 $t_u = 0.25, t_l = 0.1, \text{ num. skipped points}=0$

Gmu	t_c	probability	max. edgelenlength	mean a
1.0000000e-08	7.00000	0.44757170	11.000000	0.99967664
2.0000000e-08	4.00000	0.0020638683	14.000000	0.99862559
4.0000000e-08	3.00000	0.0000000	21.000000	0.99447207
6.0000000e-08	3.00000	0	33	0.98754092

Table 2: Unsmoothed String Map versus Gaussian Map: N=10
Minimum Edge Length: 2
 $t_u = 0.25, t_l = 0.1, \text{ skipped points}=0$

Gmu	t_c	probability	max. edgelenlength	mean a
1.0000000e-08	7.00000	0.56022527	11.000000	0.99967664
2.0000000e-08	4.00000	0.087458606	14.000000	0.99862559
4.0000000e-08	3.00000	4.8140603e-11	21.000000	0.99447207
6.0000000e-08	3.00000	0.0000000	33.000000	0.98754092

V. CONCLUSIONS AND DISCUSSION

We have developed a new program to search for cosmic strings in CMB anisotropy maps making use of the

Canny algorithm, and have tested it with simulated data corresponding to maps with specifications corresponding to those of current ground-based CMB experiments. The code contains a number of optimization parameters, and

Table 3
 Minimum Edge Length: 1
 Smoothed String Map versus Gaussian Map N=10
 $t_u = 0.25, t_l = 0.1, \text{ num. skipped points}=0$

Gmu	t_c	probability	max. edgelenh	mean a
6.0000000e-08	3.00000	0.10701445	42.000000	0.98754092
8.0000000e-08	3.00000	0.059179809	46.000000	0.97932855
9.0000000e-08	3.00000	0.00012533417	46.000000	0.97174247
1.0000000e-07	3.00000	2.4759972e-11	52.000000	0.96499435
1.5000000e-07	2.50000	0.0000000	59.000000	0.91936485

Table 4
 Minimum Edge Length: 1
 Unsmoothed String Map versus Gaussian Map: N=1
 $t_u = 0.03, t_l = 0.005, \text{ skipped points}=0$

Gmu	t_c	probability	max. edgelenh	mean a
2.0000000e-08	4.00000	0.43985131	7.0000000	0.99986506
4.0000000e-08	3.00000	0.76437603	11.000000	0.99937157
6.0000000e-08	3.00000	0.0019923380	19.000000	0.99901436
8.0000000e-08	3.00000	8.7787192e-09	28.000000	0.99816180
9.0000000e-08	3.00000	3.8369308e-13	32.000000	0.99757307

we have discussed the role of these parameters.

Our results (based on a rough optimization of the parameters) show that our algorithm has the potential to improve the bounds on the cosmic string tension from direct CMB observations by up to two orders of magnitude compared to existing limits, and by one order of magnitude from other more indirect limits. The limiting value of $G\mu$ decreases as N (the number of strings per Hubble volume per Hubble time) increases. For cosmic superstrings the intercommutation probability may be much lower than for Abelian field theory strings, thus leading to a larger value of N [56]. Hence, our method may be able to set more stringent limits of the value of $G\mu$ in the case of cosmic superstrings.⁹

A possible concern with our analysis is that our toy model of representing the effects of a string on the microwave sky introduces artificial edges. Although the presence of the central edge in the CMB pattern of a string is clearly physical, the edges perpendicular to this central edge are due to the toy model which considers finite length string segments rather than a network of infinite strings. Although the temperature perturbation clearly goes to zero at a perpendicular distance t from a string present at time t , the sharpness of the change given by [28] may be modulated by interactions between the time of formation of the string network and the time t ¹⁰. Thus, one of our simulations with N strings per Hubble volume per Hubble time may contain as many edges as a “real” string map with $4N$ strings per Hubble

volume per Hubble time. As can be seen by comparing Tables 4 and 5, the dependence of the limits on $G\mu$ on N is not large. The limit on $G\mu$ appears to scale as N^{-1} . Thus, the limit on $G\mu$ obtained from our analysis might be a factor of 3 too optimistic due to the larger number of edges. This point could also be addressed by a Canny algorithm analysis of more sophisticated string simulations, which we shall pursue as a follow-up study.

The results presented here are based on comparing simulations with and without cosmic strings of a known value of $G\mu$. However, we do not know the value of $G\mu$, and the goal of observations is to determine the value or to set limits on it. Hence, the way we plan to apply our algorithm to real data is to compare the edge histograms based on real data with those of a cosmic string plus Gaussian map with fixed $G\mu$, and varying $G\mu$, starting from the current limit for this quantity. Limits on $G\mu$ can be obtained if the histogram derived from the data is statistically different from that of a Gaussian plus strings map for the corresponding value of the normalized string tension. A candidate detection of cosmic strings would require the histogram derived from the real data to be statistically indistinguishable from that of a Gaussian plus strings map, and at the same time different from that of a pure Gaussian map. If there are indeed cosmic strings in the sky with a value of $G\mu$ for which our analysis gives a probability p that the histograms with and without strings are from the same distribution, then the probability that our statistical analysis would give a positive detection of these strings will be $1 - p$.

When applying the algorithm to real data, a serious concern is systematic errors introduced by the observing strategy - specifically lines in the maps due to the scanning strategy. In specific experiments such as the South Pole Telescope (SPT) experiment, lines introduced by the scanning will be in one specific direction, and thus the algorithm can be rendered immune to this effect by

⁹ While this manuscript was being prepared for submission, a preprint [59] appeared in which a novel method different from ours was proposed to search for cosmic strings. With this new method, improved limits on the cosmic string tension also appear to be possible.

¹⁰ We thank the Referee for raising this issue.

Table 5
 Minimum Edge Length: 1
 Unsmoothed String Map versus Gaussian Map:N=10
 $t_u = 0.25, t_l = 0.1, \text{skipped points}=2$

Gmu	t_c	probability	max. edgelenh	mean a
1.0000000e-08	7.00000	0.43783402	41.000000	0.99967664
2.0000000e-08	4.00000	0.30944903	55.000000	0.99862559
4.0000000e-08	3.00000	5.4179907e-08	139.00000	0.99447207

considering only edges which are not parallel to the direction of the scanning stripes. Foreground and instrumental noise are other important problems. Smoothing of the maps is supposed to reduce the latter problem, and the study of [48] confirms that instrumental noise such as that anticipated in the SPT telescope will not have a big effect on the power of the algorithm.

The next step of our research program will be to apply our code to existing data. The main challenge will be to take care of the systematic errors contained in the data. We plan to compare data for the actual sky map to Gaussian and Gaussian plus strings simulations. In order to put the data in a format for which a statistical analysis is possible, we will divide the sky maps into sub-maps of equal size, and treat each sub-map as a different realization of the sky. In other words, we make the ergodic hypothesis and identify ensemble and spatial averaging. Thus, if we want to compare squares of edge length 10^0 in the sky, then we need a total survey area 50 times larger in order to be able to have 50 independent data sets for the sky. We also plan to apply our code to more realistic cosmic string simulations, such as those of [54].

Acknowledgments

This work is supported in part by a NSERC Discovery Grant and by funds from the CRC Program. We are grateful to Stephen Amsel, Andrew Stewart and Eric Thewalt for many discussions on numerical issues. We also wish to thank Matt Dobbs, Aurelien Fraisse, Christophe Ringeval, and in particular Gil Holder for useful communications. R.D. would like to thank Andrew Frey for useful discussions.

VI. APPENDIX A

In this Appendix we describe the maxima doubling problem which arises in our implementation of the Canny algorithm. Let us illustrate the problem in terms of an example.

If the temperature grid points are

$$\begin{array}{cccc} 6 & 8 & 10 & 20 \\ 3 & 5 & 12 & 14 \\ 4 & 6 & 9 & 11 \end{array} \quad (28)$$

and the points are labeled starting from 0 from left to right top to bottom, then the point at grid point 5 (temperature 5) is a local maximum with gradient 7 along the 0 direction. The grid point 6 (temperature 12) is a local maximum along the 1 direction with gradient 8. There aren't any doubles in this case.

However, if we had

$$\begin{array}{cccc} 6 & 8 & 10 & 15 \\ 3 & 5 & 12 & 14 \\ 4 & 6 & 9 & 11 \end{array} \quad (29)$$

then the grid point 5 (temperature 5) is a local maximum along the 0 direction with a gradient of 7 and the grid point 6 (temperature 12) is a local maximum along the 4 direction with gradient 7. We use a sorting routine to remove the first occurrence of a gradient of 7 (index 5) as we want there to be only one local maximum at this point.

-
- [1] A. C. Davis and T. W. B. Kibble, "Fundamental cosmic strings," *Contemp. Phys.* **46**, 313 (2005) [arXiv:hep-th/0505050];
 M. Sakellariadou, "Cosmic Superstrings," arXiv:0802.3379 [hep-th].
- [2] R. Jeannerot, "A Supersymmetric SO(10) Model with Inflation and Cosmic Strings," *Phys. Rev. D* **53**, 5426 (1996) [arXiv:hep-ph/9509365];
 R. Jeannerot, J. Rocher and M. Sakellariadou, "How generic is cosmic string formation in SUSY GUTs," *Phys. Rev. D* **68**, 103514 (2003) [arXiv:hep-ph/0308134].
- [3] S. Sarangi and S. H. H. Tye, "Cosmic string production towards the end of brane inflation," *Phys. Lett. B* **536**, 185 (2002) [arXiv:hep-th/0204074].
- [4] E. Witten, "Cosmic Superstrings," *Phys. Lett. B* **153**, 243 (1985).
- [5] E. J. Copeland, R. C. Myers and J. Polchinski, "Cosmic F- and D-strings," *JHEP* **0406**, 013 (2004) [arXiv:hep-th/0312067].
- [6] J. Khoury, B. A. Ovrut, P. J. Steinhardt and N. Turok, "The ekpyrotic universe: Colliding branes and the origin of the hot big bang," *Phys. Rev. D* **64**, 123522 (2001) [arXiv:hep-th/0103239].
- [7] R. H. Brandenberger and C. Vafa, "Superstrings In The

- Early Universe,” Nucl. Phys. B **316**, 391 (1989).
- [8] A. Nayeri, R. H. Brandenberger and C. Vafa, “Producing a scale-invariant spectrum of perturbations in a Hagedorn phase of string cosmology,” Phys. Rev. Lett. **97**, 021302 (2006) [arXiv:hep-th/0511140];
R. H. Brandenberger, A. Nayeri, S. P. Patil and C. Vafa, “String gas cosmology and structure formation,” arXiv:hep-th/0608121.
- [9] T. W. B. Kibble, “Phase Transitions In The Early Universe,” Acta Phys. Polon. B **13**, 723 (1982);
T. W. B. Kibble, “Some Implications Of A Cosmological Phase Transition,” Phys. Rept. **67**, 183 (1980).
- [10] A. Vilenkin and E.P.S. Shellard; *Cosmic Strings and Other Topological Defects*, (Cambridge Univ. Press, Cambridge, 1994).
- [11] M. B. Hindmarsh and T. W. Kibble, “Cosmic strings,” Rept. Prog. Phys. **58**, 477 (1995) [arXiv:hep-ph/9411342].
- [12] R. H. Brandenberger, “Topological defects and structure formation,” Int. J. Mod. Phys. A **9**, 2117 (1994) [arXiv:astro-ph/9310041].
- [13] T. W. B. Kibble, “Topology Of Cosmic Domains And Strings,” J. Phys. A **9**, 1387 (1976);
Y. B. Zeldovich, “Cosmological fluctuations produced near a singularity,” Mon. Not. Roy. Astron. Soc. **192**, 663 (1980);
A. Vilenkin, “Cosmological Density Fluctuations Produced By Vacuum Strings,” Phys. Rev. Lett. **46**, 1169 (1981) [Erratum-ibid. **46**, 1496 (1981)].
- [14] A. Vilenkin, “Cosmic Strings And Domain Walls,” Phys. Rept. **121**, 263 (1985).
- [15] A. Albrecht and N. Turok, “Evolution Of Cosmic Strings,” Phys. Rev. Lett. **54**, 1868 (1985).
- [16] D. P. Bennett and F. R. Bouchet, “Evidence For A Scaling Solution In Cosmic String Evolution,” Phys. Rev. Lett. **60**, 257 (1988).
- [17] B. Allen and E. P. S. Shellard, “Cosmic String Evolution: A Numerical Simulation,” Phys. Rev. Lett. **64**, 119 (1990).
- [18] G. Vincent, N. D. Antunes and M. Hindmarsh, “Numerical simulations of string networks in the Abelian-Higgs model,” Phys. Rev. Lett. **80**, 2277 (1998) [arXiv:hep-ph/9708427].
- [19] V. Vanchurin, K. D. Olum and A. Vilenkin, “Scaling of cosmic string loops,” Phys. Rev. D **74**, 063527 (2006) [arXiv:gr-qc/0511159].
- [20] C. J. A. Martins and E. P. S. Shellard, “Fractal properties and small-scale structure of cosmic string networks,” Phys. Rev. D **73**, 043515 (2006) [arXiv:astro-ph/0511792].
- [21] C. Ringeval, M. Sakellariadou and F. Bouchet, “Cosmological evolution of cosmic string loops,” JCAP **0702**, 023 (2007) [arXiv:astro-ph/0511646].
- [22] J. N. Moore and E. P. S. Shellard, “On the evolution of abelian-Higgs string networks,” arXiv:hep-ph/9808336.
- [23] J. Polchinski, “Cosmic String Loops and Gravitational Radiation,” arXiv:0707.0888 [astro-ph].
- [24] H. B. Nielsen and P. Olesen, “Vortex-Line Models For Dual Strings,” Nucl. Phys. B **61**, 45 (1973).
- [25] N. Turok and R. H. Brandenberger, “Cosmic Strings And The Formation Of Galaxies And Clusters Of Galaxies,” Phys. Rev. D **33**, 2175 (1986);
H. Sato, “Galaxy Formation by Cosmic Strings,” Prog. Theor. Phys. **75**, 1342 (1986);
A. Stebbins, “Cosmic Strings and Cold Matter”, Ap. J. (Lett.) **303**, L21 (1986).
- [26] N. Kaiser and A. Stebbins, “Microwave Anisotropy Due To Cosmic Strings,” Nature **310**, 391 (1984).
- [27] A. Vilenkin, “Gravitational Field Of Vacuum Domain Walls And Strings,” Phys. Rev. D **23**, 852 (1981).
- [28] J. C. R. Magueijo, “Inborn metric of cosmic strings,” Phys. Rev. D **46**, 1368 (1992).
- [29] A. Kosowsky [the ACT Collaboration], “The Atacama Cosmology Telescope Project: A Progress Report,” New Astron. Rev. **50**, 969 (2006) [arXiv:astro-ph/0608549].
- [30] J. E. Ruhl *et al.* [The SPT Collaboration], “The South Pole Telescope,” Proc. SPIE Int. Soc. Opt. Eng. **5498**, 11 (2004) [arXiv:astro-ph/0411122].
- [31] F. Villa *et al.* [The Planck Collaboration], “The Planck Telescope,” AIP Conf. Proc. **616**, 224 (2002) [arXiv:astro-ph/0112173];
J. Tauber (on behalf of ESA and the Planck Science Collaboration), “The Planck Mission”, Advances in Space Research (2004).
- [32] R. K. Sachs and A. M. Wolfe, “Perturbations of a cosmological model and angular variations of the microwave background,” Astrophys. J. **147**, 73 (1967).
- [33] A. Albrecht, D. Coulson, P. Ferreira and J. Magueijo, “Causality and the microwave background,” Phys. Rev. Lett. **76**, 1413 (1996) [arXiv:astro-ph/9505030].
- [34] L. Perivolaropoulos, “Spectral Analysis Of Microwave Background Perturbations Induced By Cosmic Strings,” Astrophys. J. **451**, 429 (1995) [arXiv:astro-ph/9402024].
- [35] J. Magueijo, A. Albrecht, D. Coulson and P. Ferreira, “Doppler peaks from active perturbations,” Phys. Rev. Lett. **76**, 2617 (1996) [arXiv:astro-ph/9511042].
- [36] U. L. Pen, U. Seljak and N. Turok, “Power spectra in global defect theories of cosmic structure formation,” Phys. Rev. Lett. **79**, 1611 (1997) [arXiv:astro-ph/9704165].
- [37] R. A. Sunyaev and Y. B. Zeldovich, “Small scale fluctuations of relic radiation,” Astrophys. Space Sci. **7**, 3 (1970).
- [38] P. D. Mauskopf *et al.* [Boomerang Collaboration], “Measurement of a Peak in the Cosmic Microwave Background Power Spectrum from the North American test flight of BOOMERANG,” Astrophys. J. **536**, L59 (2000) [arXiv:astro-ph/9911444].
- [39] C. L. Bennett *et al.*, “First Year Wilkinson Microwave Anisotropy Probe (WMAP) Observations: Preliminary Maps and Basic Results,” Astrophys. J. Suppl. **148**, 1 (2003) [arXiv:astro-ph/0302207].
- [40] L. Pogosian, S. H. H. Tye, I. Wasserman and M. Wyman, “Observational constraints on cosmic string production during brane inflation,” Phys. Rev. D **68**, 023506 (2003) [Erratum-ibid. D **73**, 089904 (2006)] [arXiv:hep-th/0304188];
M. Wyman, L. Pogosian and I. Wasserman, “Bounds on cosmic strings from WMAP and SDSS,” Phys. Rev. D **72**, 023513 (2005) [Erratum-ibid. D **73**, 089905 (2006)] [arXiv:astro-ph/0503364];
A. A. Fraisse, “Limits on Defects Formation and Hybrid Inflationary Models with Three-Year WMAP Observations,” JCAP **0703**, 008 (2007) [arXiv:astro-ph/0603589];
U. Seljak, A. Slosar and P. McDonald, “Cosmological parameters from combining the Lyman-alpha forest with CMB, galaxy clustering and SN constraints,” JCAP

- 0610**, 014 (2006) [arXiv:astro-ph/0604335];
 N. Bevis, M. Hindmarsh, M. Kunz and J. Urrestilla, “CMB power spectrum contribution from cosmic strings using field-evolution simulations of the Abelian Higgs model,” *Phys. Rev. D* **75**, 065015 (2007) [arXiv:astro-ph/0605018];
 N. Bevis, M. Hindmarsh, M. Kunz and J. Urrestilla, “Fitting CMB data with cosmic strings and inflation,” arXiv:astro-ph/0702223.
 R. A. Battye, B. Garbrecht and A. Moss, “Constraints on supersymmetric models of hybrid inflation,” *JCAP* **0609**, 007 (2006) [arXiv:astro-ph/0607339];
 R. A. Battye, B. Garbrecht, A. Moss and H. Stoica, “Constraints on Brane Inflation and Cosmic Strings,” *JCAP* **0801**, 020 (2008) [arXiv:0710.1541 [astro-ph]].
- [41] F. R. Bouchet and D. P. Bennett, “Does The Millisecond Pulsar Constrain Cosmic Strings?,” *Phys. Rev. D* **41**, 720 (1990).
- [42] V. M. Kaspi, J. H. Taylor and M. F. Ryba, “High - precision timing of millisecond pulsars. 3: Long - term monitoring of PSRs B1855+09 and B1937+21,” *Astrophys. J.* **428**, 713 (1994);
 S. E. Thorsett and R. J. Dewey, “Pulsar timing limits on very low frequency stochastic gravitational radiation,” *Phys. Rev. D* **53**, 3468 (1996);
 M. P. McHugh, G. Zalamansky, F. Vernotte and E. Lantz, “Pulsar Timing And The Upper Limits On A Gravitational Wave Background: A Bayesian Approach,” *Phys. Rev. D* **54**, 5993 (1996);
 A. N. Lommen, “New limits on gravitational radiation using pulsars,” arXiv:astro-ph/0208572;
 F. A. Jenet *et al.*, “Upper bounds on the low-frequency stochastic gravitational wave background from pulsar timing observations: Current limits and future prospects,” *Astrophys. J.* **653**, 1571 (2006) [arXiv:astro-ph/0609013].
- [43] R. Moessner, L. Perivolaropoulos and R. H. Brandenberger, “A Cosmic string specific signature on the cosmic microwave background,” *Astrophys. J.* **425**, 365 (1994) [arXiv:astro-ph/9310001].
- [44] A. S. Lo and E. L. Wright, “Signatures of cosmic strings in the cosmic microwave background,” arXiv:astro-ph/0503120.
- [45] E. Jeong and G. F. Smoot, “Search for cosmic strings in CMB anisotropies,” *Astrophys. J.* **624**, 21 (2005) [arXiv:astro-ph/0406432];
 E. Jeong and G. F. Smoot, “The Validity of the Cosmic String Pattern Search with the Cosmic Microwave Background,” arXiv:astro-ph/0612706.
- [46] S. Amsel, J. Berger and R. H. Brandenberger, “Detecting Cosmic Strings in the CMB with the Canny Algorithm,” *JCAP* **0804**, 015 (2008) [arXiv:0709.0982 [astro-ph]].
- [47] J. Canny, “A computational approach to edge detection,” *IEEE Trans. Pattern Analysis and Machine Intelligence* **8**, 679 (1986).
- [48] A. Stewart and R. Brandenberger, “Edge Detection, Cosmic Strings and the South Pole Telescope,” arXiv:0809.0865 [astro-ph].
- [49] M. J. White, J. E. Carlstrom and M. Dragovan, “Interferometric Observation of Cosmic Microwave Background Anisotropies,” *Astrophys. J.* **514**, 12 (1999) [arXiv:astro-ph/9712195].
- [50] A. Lewis, A. Challinor and A. Lasenby, “Efficient Computation of CMB anisotropies in closed FRW models,” *Astrophys. J.* **538**, 473 (2000) [arXiv:astro-ph/9911177].
- [51] U. Seljak and M. Zaldarriaga, “A Line of Sight Approach to Cosmic Microwave Background Anisotropies,” *Astrophys. J.* **469**, 437 (1996) [arXiv:astro-ph/9603033].
- [52] C. l. Kuo *et al.* [ACBAR collaboration], “High Resolution Observations of the CMB Power Spectrum with ACBAR,” *Astrophys. J.* **600**, 32 (2004) [arXiv:astro-ph/0212289].
- [53] C. L. Reichardt *et al.*, “High resolution CMB power spectrum from the complete ACBAR data set,” arXiv:0801.1491 [astro-ph].
- [54] A. A. Fraisse, C. Ringeval, D. N. Spergel and F. R. Bouchet, “Small-Angle CMB Temperature Anisotropies Induced by Cosmic Strings,” arXiv:0708.1162 [astro-ph].
- [55] L. Perivolaropoulos, “COBE versus cosmic strings: An Analytical model,” *Phys. Lett. B* **298**, 305 (1993) [arXiv:hep-ph/9208247];
 L. Perivolaropoulos, “Statistics of microwave fluctuations induced by topological defects,” *Phys. Rev. D* **48**, 1530 (1993) [arXiv:hep-ph/9212228].
- [56] J. Polchinski, “Introduction to cosmic F- and D-strings,” arXiv:hep-th/0412244.
- [57] J. H. Traschen, N. Turok and R. H. Brandenberger, “Microwave Anisotropies from Cosmic Strings,” *Phys. Rev. D* **34**, 919 (1986).
- [58] E. Komatsu *et al.* [WMAP Collaboration], “Five-Year Wilkinson Microwave Anisotropy Probe Observations: Cosmological Interpretation,” arXiv:0803.0547 [astro-ph].
- [59] D. K. Hammond, Y. Wiaux and P. Vanderghelynst, “Wavelet domain Bayesian denoising of string signal in the cosmic microwave background,” arXiv:0811.1267 [astro-ph].